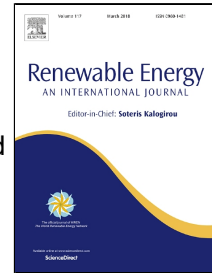


# Accepted Manuscript

Control concepts of a radiant wall working as thermal energy storage for peak load shifting of a heat pump coupled to a PV array



Joaquim Romani, Martin Belusko, Alemu Alemu, Luisa F. Cabeza, Alvaro de Gracia, Frank Bruno

PII: S0960-1481(17)31137-0  
DOI: 10.1016/j.renene.2017.11.036  
Reference: RENE 9438  
To appear in: *Renewable Energy*  
Received Date: 17 July 2017  
Revised Date: 10 November 2017  
Accepted Date: 13 November 2017

Please cite this article as: Joaquim Romani, Martin Belusko, Alemu Alemu, Luisa F. Cabeza, Alvaro de Gracia, Frank Bruno, Control concepts of a radiant wall working as thermal energy storage for peak load shifting of a heat pump coupled to a PV array, *Renewable Energy* (2017), doi: 10.1016/j.renene.2017.11.036

This is a PDF file of an unedited manuscript that has been accepted for publication. As a service to our customers we are providing this early version of the manuscript. The manuscript will undergo copyediting, typesetting, and review of the resulting proof before it is published in its final form. Please note that during the production process errors may be discovered which could affect the content, and all legal disclaimers that apply to the journal pertain.

**Highlights for:** Control concepts of a radiant wall working as thermal energy storage for peak load shifting of a heat pump coupled to a PV array

- A validated model was used for studying control concepts of a radiant wall
- Storing energy in the radiant wall results in a higher energy use of the heat pump
- Self-consumption of PV panels output minimizes imported energy from the grid
- Investment in PV panels is only useful with specific “solar” control strategies



FVM	Finite volume model
COP	Coefficient of performance

33

Parameters		Sub-index	
T	Temperature (°C)	as	Assumed
$P_{PV}$	Output power of PV array (W)	calc	Calculated
R	Thermal resistances ( $K \cdot W^{-1}$ )	i	Surface
$\epsilon$	Emissivity (-)	i-j	Heat transfer between surfaces
A	Area ( $m^2$ )	rad	Radiation
G	View factor (-)	conv	Convection
q	Heat flux (W)	load	Cooling load
X	Thermal resistances matrix ( $W \cdot K^{-1}$ )	inv	Inverse matrix
Y	Temperature gradient matrix (K)	(i,j)	Position in the matrix
Z	Heat flux matrix (W)	out	Outdoor
I	Infiltrations (% of air exchange per time step)	in	Indoor
$\rho$	Density ( $kg \cdot m^{-3}$ )	star	Star node
$c_p$	Specific heat capacity ( $J \cdot kg^{-1} \cdot K^{-1}$ )		
V	Volume ( $m^3$ )		
$\Delta t$	Time step (s)		
t	Time (s)		
h	Convective heat transfer coefficient ( $W \cdot m^{-2} \cdot K^{-1}$ )		
rf	Relaxation factor		

34

## 35 1. Introduction

36

37 Buildings are widely known as global major energy consumers and greenhouse gas emitters, with  
 38 32 % of global energy use [1] and 36 % of overall CO<sub>2</sub> emissions [2]. This issue is tackled by the  
 39 European Directive 2010/31/EU [3] and it is also present in Paris COP 21 agreements [4]. The  
 40 first step to solve this problem requires improving energy efficiency in buildings by improvement  
 41 of envelopes, management of solar gains, and reduction of internal loads, among others. However,  
 42 the final objective is to achieve net-zero energy buildings or even net-positive energy buildings  
 43 [3], meaning that buildings should at least produce the same energy they consume. This implies

44 integration of renewable energy into buildings, however the mismatch between availability of  
45 renewable energy and building energy demand profiles also requires energy storage systems.

46

47 Thermally activated building systems (TABS) have been widely studied for their potential to  
48 reduce energy use of buildings for space heating and cooling [5-8]. TABS consist of pipes or  
49 ducts embedded into the building structure, such as floors, ceilings, walls, and in-floor slabs. As  
50 a result, TABS make use of the availability of big internal surface in the building, which allows  
51 fulfilling the heating or cooling demands at reduced gradients between the fluid supply  
52 temperature and the indoor space temperature. As a result, TABS can operate with lower supply  
53 temperature for heating or higher supply temperature for cooling [5]. This is useful to increase  
54 the efficiency of heating and cooling systems or to integrate renewable energy sources, for  
55 example, free-cooling with ground heat exchangers [9] or night cool air [10]. Moreover, the fluid  
56 circulating through the pipes or ducts directly exchanges heat with the building structure and,  
57 thus, the building thermal mass is actively used for energy storage. Consequently, TABS can be  
58 considered as a short term, sensible, and low temperature thermal energy storage (TES)  
59 technology characterized as being actively charged and passively discharged. The storage  
60 capacity of TABS further increases their capability for integration of renewable energies through  
61 peak load shifting.

62

63 A promising system for integration of renewable energy in heating and cooling consists of  
64 photovoltaic panel (PV) arrays feeding heat pumps coupled to a TES system. The solar power  
65 produced is used for heating, cooling, or other electrical-consuming appliances. However, when  
66 PV output is higher than the building energy demand, the excess energy is not sold to the grid but  
67 used to charge a TES through the heat pump. Regarding this system working in heating mode, a  
68 simulation study of photovoltaic thermal array (PVT) coupled to a ground source heat pump and  
69 a water tank showed that the system provided 96 % of the electrical demand and fulfilled all heat  
70 demand [11]. A similar project determined the PV surface required to achieve a net-positive  
71 building in a system without a storage tank but a radiant floor [12]. The control of this system  
72 was also studied. A model predictive control (MPC) showed an improved performance in a system  
73 using high-mass radiant floor together with a TES tank [13]. The same control model showed a  
74 45 % energy saving in a similar set-up [14]. This system was also applied for cooling, showing  
75 different economic opportunities in Brazil [15]. Additionally, its implementation into industrial  
76 buildings was also studied, with results indicating economic potential of exploiting PV output or  
77 off-peak periods [16]. All of these studies aimed towards net-zero or net-positive energy buildings  
78 and most considered some kind of TES [11,13,14,16]. However, most of them considered that the  
79 PV electrical power output fulfilled the electricity demand by using the grid as energy storage.

80 Furthermore, several studies considered some kind of TABS in the form of radiant heating floors  
81 [11-14], but only one considered it as a TES system [14].

82

83 A challenging topic to overcome for a wide implementation of TABS is the control. The  
84 management of the low response time and the peak load shifting capability require control  
85 strategies that take into account the dynamics of the system. Moreover, controlling TABS implies  
86 defining the supply temperature, the flow, and the ON/OFF criterion, which involves defining the  
87 duration of the active period. Usually the supply temperature is regulated by a heating/cooling  
88 curve dependant on outdoor conditions [17], although constant supply temperature is also used.  
89 On the other side, the simplest strategy for ON/OFF are set-back controls, in which a set-point  
90 temperature is maintained with a dead band regulating the temperature at which the system turns  
91 ON or OFF [18]. Both heating/cooling curves and set-back are reliable and robust controls,  
92 however, optimization of TABS operation requires more advanced controls. As a result, TABS  
93 were studied coupled to gain scheduling control (GSC) [19], pulse width modulation (PWM) [20],  
94 adaptive predictive control [21], and MPC [13,22], among others, all showing improved  
95 performance compared to common base case controls. Finally, MPC was highlighted as a control  
96 scheme with good potential for optimizing TABS operation, although further research is needed  
97 [8].

98

99 The current paper presents a study of the control concepts for a system consisting of a radiant  
100 wall supplied by a heat pump coupled to a PV array. The main objective was to minimize the cost  
101 for space cooling of a building, and thus the peak load shifting capacity of the radiant wall was  
102 used for operation during off-peak periods or for charging during periods with availability of solar  
103 energy. Here, the only storage system was the radiant wall itself, which was considered as a short  
104 term TES. The research was carried out by simulating the performance of the system under  
105 different control concepts which gave guidelines of the best way to operate the system for  
106 reducing cooling cost.

107

108 In order to develop the study, a numerical model was developed for a simplified cubicle exposed  
109 to outdoor conditions. These approach was based in previous experimental research on radiant  
110 wall cubicle, which showed good energy savings potential and peak load shifting capability  
111 [24,25]. From this experimental research, a numerical model of the radiant wall was validated  
112 [26] and then implemented in the current research.

113

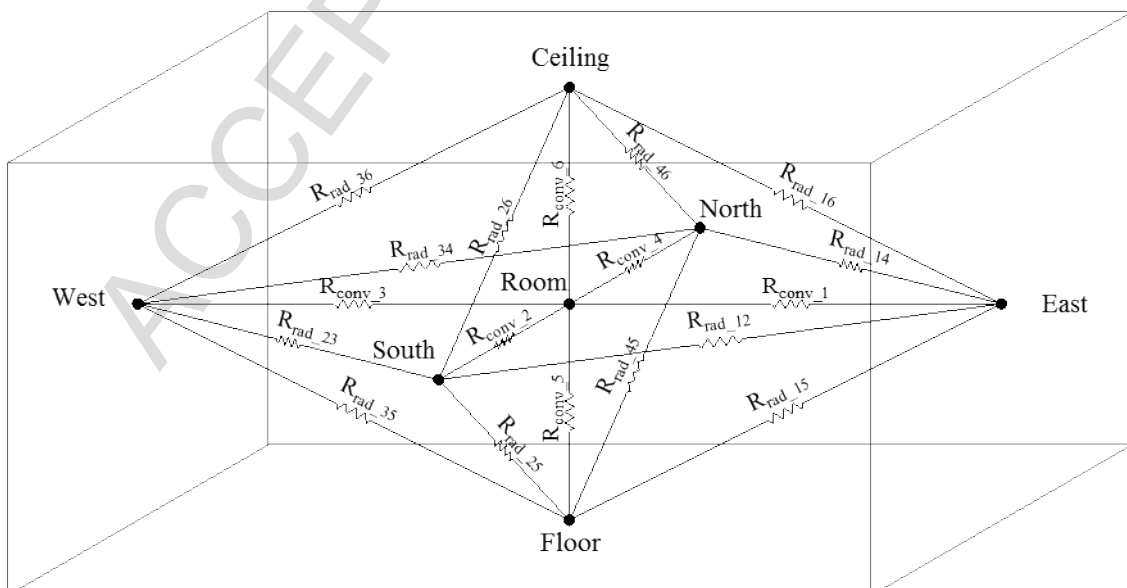
## 114 **2. Model description**

115

116 In previous research, a 2D transient finite volume model of a radiant wall was developed and  
 117 experimentally validated [26]. However, this model only described the behaviour of the radiant  
 118 wall, which required, among other inputs, the indoor temperature. In order to study control  
 119 strategies a cooling demand was required, consequently a building model had to be implemented.  
 120 In the research of the current paper a simplified model of a cubicle, a room without openings, was  
 121 used. This had internal size of 5.25 x 2.7 x 2.7 m (surface of 14.175 m<sup>2</sup>) with radiant walls in all  
 122 the walls, and without windows. All the walls were exposed to outdoor conditions. These  
 123 approach was based on the knowledge obtained in previous experimental research of a radiant  
 124 wall cubicle [24,25]. The collected data was used for verifying the reliability of the room model.  
 125  
 126 The following sections describe the details of the cubicle model, the associated components, and  
 127 the calculation algorithms.  
 128

### 129 2.1. Cubicle model

130  
 131 The cubicle was modelled using a six surface star-network according to the methodology  
 132 proposed by Seem [28]. This modelling simplifies actual radiation and convection heat transfer  
 133 processes in the room avoiding the manipulation of polynomial matrices required when view  
 134 factors are used to model long-wave radiation. Seem [28] presented a computationally easy  
 135 method for transforming the view factor scheme, shown in Figure 1, into the star-network scheme  
 136 shown in Figure 2. The star node represents a fictitious temperature that channels the radiation  
 137 heat transfer between surfaces and the convection heat transfer between the surfaces and the  
 138 indoor air.  
 139

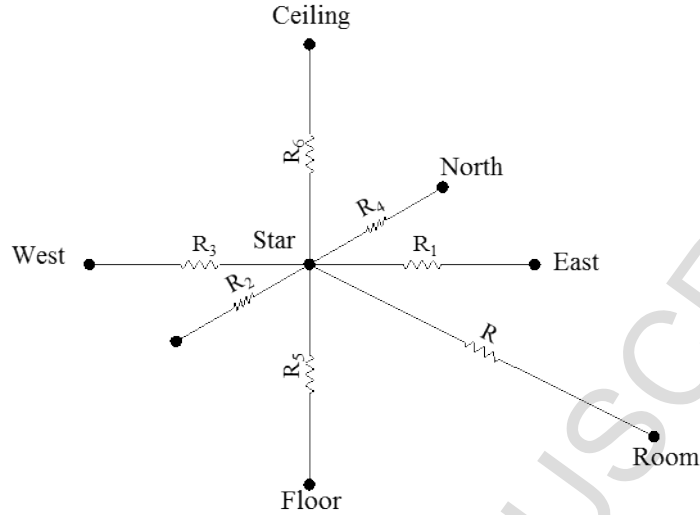


140

141

142 Figure 1. View factors heat transfer scheme (note radiation resistances between opposite surfaces could  
 143 not be represented)

144



145

146

Figure 2. Star-network scheme for six surfaces

147

148 The view factor matrix convection resistances ( $R_{conv,i}$ ) were calculated using the convection  
 149 factors of UNE-EN ISO 6946 for indoor surfaces; note that this standard proposes a mixed  
 150 convection and radiation factor, but in this paper  $R_{i,c}$  was calculated only with the convection  
 151 part, as the model considered radiation independently.

152

153 The radiation between surfaces was represented with  $R_{rad,i-j}$ , which was calculated with  
 154 equation (1) [29].

155

$$156 \quad R_{rad,i-j} = \frac{1}{\varepsilon_i \cdot A_i \cdot G_{i-j} \cdot \sigma \cdot 4 \cdot \bar{T}}$$

157 (Eq. 1)

158

159 where  $\varepsilon_i$  was emissivity,  $A_i$  area,  $G_{i-j}$  view factor between surfaces,  $\sigma$  Stefan-Boltzmann  
 160 constant, and  $\bar{T}$  was calculated with equation (2). Note that actual view factors were used.

161

$$162 \quad \bar{T} = (T_i + T_j) \cdot (T_i^2 + T_j^2)$$

163 (Eq. 2)

164

165 According to Seem, the energy balances on each surface and in the room could be combined into  
 166 matrix equations with the following form:

167

168  $X \cdot Y = Z$

169 (Eq. 3)

170

171 where Y and Z are the temperature gradient and heat flux matrixes respectively, which are shown  
 172 in Table 1. On the other side, X matrix is conductivity matrix and is presented in Table 2.

173

174

Table 1. Y and Z matrixes

Y=	$(T_1 - T_{in})$	Z=	$-q_1$
	$(T_2 - T_{in})$		$-q_2$
	$(T_3 - T_{in})$		$-q_3$
	$(T_4 - T_{in})$		$-q_4$
	$(T_5 - T_{in})$		$-q_5$
	$(T_6 - T_{in})$		$-q_6$
	$q_{load}$		$0$

Table 2. Matrix X

$-\left(\sum_{\substack{j=1 \\ j \neq 1}}^6 \frac{1}{R_{rad,1-j}}\right) - R_{conv,1}$	$\frac{1}{R_{rad,1-2}}$	$\frac{1}{R_{rad,1-3}}$	$\frac{1}{R_{rad,1-4}}$	$\frac{1}{R_{rad,1-5}}$	$\frac{1}{R_{rad,1-6}}$	$\frac{1}{R_{conv,1}}$
$\frac{1}{R_{rad,2-1}}$	$-\left(\sum_{\substack{j=1 \\ j \neq 1}}^6 \frac{1}{R_{rad,2-j}}\right) - R_{conv,2}$	$\frac{1}{R_{rad,2-3}}$	$\frac{1}{R_{rad,2-4}}$	$\frac{1}{R_{rad,2-5}}$	$\frac{1}{R_{rad,2-6}}$	$\frac{1}{R_{conv,2}}$
$\frac{1}{R_{rad,3-1}}$	$\frac{1}{R_{rad,3-2}}$	$-\left(\sum_{\substack{j=1 \\ j \neq 1}}^6 \frac{1}{R_{rad,3-j}}\right) - R_{conv,3}$	$\frac{1}{R_{rad,3-4}}$	$\frac{1}{R_{rad,3-5}}$	$\frac{1}{R_{rad,3-6}}$	$\frac{1}{R_{conv,3}}$
$\frac{1}{R_{rad,4-1}}$	$\frac{1}{R_{rad,4-2}}$	$\frac{1}{R_{rad,4-3}}$	$-\left(\sum_{\substack{j=1 \\ j \neq 1}}^6 \frac{1}{R_{rad,4-j}}\right) - R_{conv,4}$	$\frac{1}{R_{rad,4-5}}$	$\frac{1}{R_{rad,4-6}}$	$\frac{1}{R_{conv,4}}$
$\frac{1}{R_{rad,5-1}}$	$\frac{1}{R_{rad,5-2}}$	$\frac{1}{R_{rad,5-3}}$	$\frac{1}{R_{rad,5-4}}$	$-\left(\sum_{\substack{j=1 \\ j \neq 1}}^6 \frac{1}{R_{rad,5-j}}\right) - R_{conv,5}$	$\frac{1}{R_{rad,5-6}}$	$\frac{1}{R_{conv,5}}$
$\frac{1}{R_{rad,6-1}}$	$\frac{1}{R_{rad,6-2}}$	$\frac{1}{R_{rad,6-3}}$	$\frac{1}{R_{rad,6-4}}$	$\frac{1}{R_{rad,6-5}}$	$-\left(\sum_{\substack{j=1 \\ j \neq 1}}^6 \frac{1}{R_{rad,6-j}}\right) - R_{conv,6}$	$\frac{1}{R_{conv,6}}$
0	0	0	0	0	0	-1

178 Finally, according to the method, the resistances of the star-network were calculated with equation  
179 4 and equation 5:

180

$$181 \quad R = \frac{\sum_{j=2}^N \sum_{i=1}^{j-1} \frac{R_{i-r} + R_{j-r} - R_{i-j}}{R_{i-j}^3}}{\sum_{j=2}^N \sum_{i=1}^{j-1} \frac{1}{R_{i-j}^3}}$$

182 (Eq. 4)

183

$$184 \quad R_i = R_{i-r} - R$$

185 (Eq. 5)

186

187 where  $R_{i-r}$  and  $R_{i-j}$  were obtained from the inverse matrix of X as shown in equation 6 and  
188 equation 7, respectively:

189

$$190 \quad R_{i-r} = -x_{(i,i),inv}$$

191 (Eq. 6)

192

$$193 \quad R_{i-j} = x_{(i,j),inv} + x_{(j,i),inv} - x_{(i,i),inv} - x_{(j,j),inv}$$

194 (Eq. 7)

195

196 Finally,  $q_{load}$  accounted for the accumulated heat in the room air plus the internal loads and the  
197 infiltration losses, as presented in equation 8:

198

$$199 \quad q_{load} = \rho \cdot cp \cdot V \cdot \frac{T_{in} - T_{in}^{t-1}}{\Delta t} + I \cdot \rho \cdot cp \cdot V \cdot (T_{in} - T_{out}) - q_{in}$$

200 (Eq. 8)

201

202 where  $I$  was infiltration in air changes per time step and  $q_{in}$  the internal gains. Then the  $q_{load}$   
203 matches with the heat flux between star node and indoor air node, as shown in equation 9.

$$204 \quad q_{load} = \frac{(T_{in} - T_{star})}{R}$$

205

206 (Eq. 9)

207

208

209 The resistance values were calculated at each iteration as they depend on temperature. Once those  
 210 were calculated, the star temperature ( $T_{star}$ ) and the indoor temperature ( $T_{in}$ ) were calculated  
 211 according to the energy balances. The input values were the temperatures of the indoor surfaces,  
 212 the outdoor temperature, the internal gains, and the indoor temperature of the previous step. The  
 213 heat flow on each surface was used to verify the energy balance of the room model and to compare  
 214 it to the energy balances of the walls.

215

## 216 2.2. *Radiant walls model*

217

218 The radiant wall was composed of a 195 mm thick brick, 60 mm expanded polystyrene insulation,  
 219 and a finishing layer of 5 mm fibrocement board on the outdoor surface, which resulted in a  
 220 steady-state transmittance (U-value) of  $0.5 \text{ W}\cdot\text{m}^{-2}\cdot\text{K}^{-1}$ . The radiant system was obtained by 16  
 221 mm diameter pipes embedded spaced 150 mm and 36 mm deep from the indoor surface of the  
 222 wall.

223

224 The radiant walls are modelled with a 2D transient FVM model described in Romaní et al. [26].  
 225 However, the boundary conditions on the indoor surface of the radiant wall model were not  
 226 compatible with the requirements of the cubicle model. The FVM of the radiant wall model used  
 227 the combined radiation and convection heat transfer coefficient obtained according to UNE-EN  
 228 ISO 6946 [27], in which the convection heat calculated using the newton equation accounts for  
 229 both convection and radiation, as shown in equation (10) where  $h_c$  was a constant that depended  
 230 on the orientation of the surface and the heat flux,  $\varepsilon$  was the emissivity, and  $T_m$  was the average  
 231 thermodynamic temperature on the surface. In contrast, the star-network model of the room takes  
 232 into account the actual radiation heat transfer between the surfaces, by taking in account the view  
 233 factors. Moreover, once transformed to star-network, the surfaces of the room model exchange  
 234 heat with the star node, while the FVM exchanges heat with the indoor temperature.

235

$$236 \quad h_{comb} = h_c + \varepsilon \cdot 4 \cdot \sigma \cdot T_m^3$$

237 (Eq. 10)

238

239 In order to match the cubicle model, the boundary condition on the indoor surface of the wall was  
 240 modified to a heat exchange with  $T_{star}$  with a heat transfer equivalent to the surface resistances  
 241 of each wall in the star-network, as shown in equation (11):

242

$$243 \quad h_{int} = \frac{1}{R_i \cdot A_i}$$

244 (Eq. 11)

245

246 The cubicle model assumed average surface temperature for each wall. However, the FVM model  
247 calculated a temperature profile on the indoor surfaces. Therefore, the results of the radiant wall  
248 temperature were summarized to an average surface temperature, in which each node temperature  
249 was weighted according to its surface.

250

251 Moreover, as the room model needed uniform surfaces, the whole surface of the radiant walls was  
252 considered to have embedded pipes. In order to match this assumption, the length of piping in the  
253 radiant walls was calculated proportionally to the wall surface area. The FVM had a definite  
254 pipes-to-wall ratio, which was used to calculate the total pipe length. This calculation was  
255 required to accurately obtain the heat flux required to the heat pump in order to achieve the  
256 adequate cooling at the walls surface.

257

### 258 2.3. Floor and roof model

259

260 The floor was modelled together with the ground in a mixed FVM mesh. The ground was  
261 modelled as 1D, with the under-ground boundary temperature calculated with Joan & Baggs  
262 equation [31]. Then, the concrete base of the cubicle was modelled as 2D, representing the slab  
263 from North to South. The boundary conditions considered that all the nodes at the bottom of the  
264 slab exchanged heat to the single node of the ground. The nodes exposed to outdoors had  
265 convective heat exchange with outdoor air. Furthermore, the horizontal surface exposed to  
266 outdoor on the south had incident solar radiation, while the north surface was considered to be in  
267 the shadow. On the other side, the nodes below the walls considered this boundary as adiabatic,  
268 as no heat exchange with walls was considered. Finally, nodes on the indoor surface exchanged  
269 heat with  $T_{star}$  in the same way as the walls, and thus using also equation 10. Furthermore, for  
270 the calculation of the room temperature, the floor temperature was considered as a uniform value  
271 equivalent to the average node temperatures, weighted by surface area.

272

273

274 The roof model consisted in 1D transient FVM. The model was solved explicitly to reduce the  
275 computational effort. On the outdoor surface the model considered convective heat exchange with  
276 outdoor air, incident horizontal solar radiation, and long-wave heat exchange with the sky. The  
277 long wave radiation was calculated with the radiosity and irradiosity method, assuming sky

278 temperature according to the Swinback correlation [30]. On the indoor surface the roof exchanges  
 279 heat against  $T_{star}$  with a heat transfer coefficient obtained from the star network ( $R_i$ ).

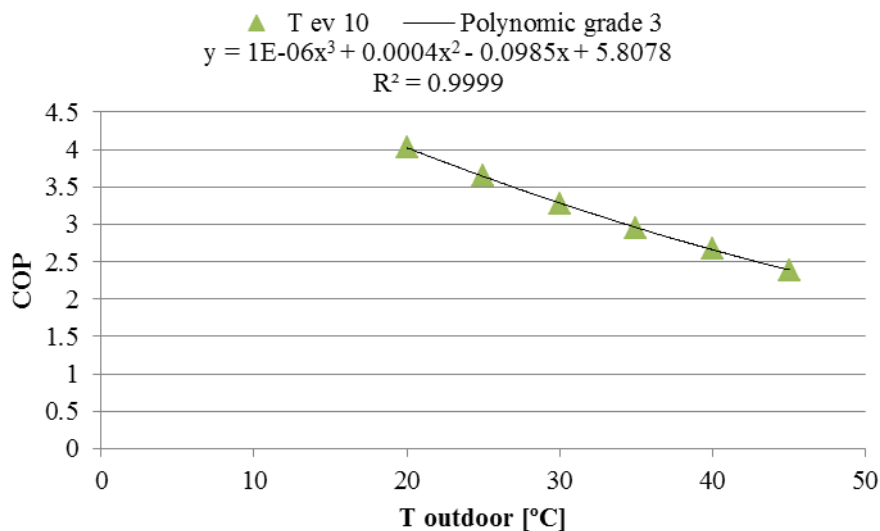
280

#### 281 2.4. Heat pump model

282

283 Several assumptions were taken into consideration for the heat pump modelling. First, the supply  
 284 temperature to the walls was constant at 15 °C, assuming a temperature gradient in the evaporator  
 285 of 5 K, which resulted in an evaporator temperature of 10 °C. With these assumptions, the COP  
 286 of the heat pump was modelled as a regression curve of the values provided by a manufacturer  
 287 [32] for a LH33E/2GES-2Y-40S compressor. The COP is provided depending on the outdoor  
 288 temperature at a specific evaporator temperature, including the fan power. The regression curve  
 289 obtained is shown in Figure 3. Finally, the total electrical energy use of the heat pump was  
 290 calculated with the calculated COP and the heat flux in the radiant walls at each time step.

291



292

293

Figure 3. Heat pump COP curve at evaporator temperature 10 °C

294

#### 295 2.5. Model of PV panels

296

297 The PV panels were simplified by assuming a constant efficiency of 15 %, and thus the electricity  
 298 supplied was a constant fraction of the incident global solar radiation. This study considered 6  
 299 panels of 1.68 m<sup>2</sup> each, placed horizontally. The total nominal power of installed PV was  
 300 equivalent to 1512 W.

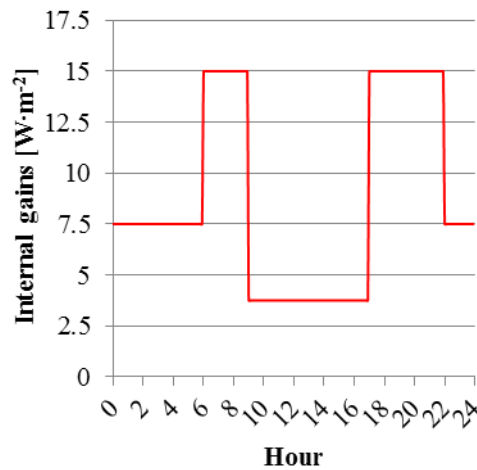
301

302      2.6. *Internal gains*

303

304      The internal gains introduced in the model represent domestic occupancy. It takes into account  
 305      the high activity periods of occupants in the early morning and afternoon, the occupancy with low  
 306      activity at night, and non-occupancy during the day. Minimum internal loads were used during  
 307      non-occupancy in order to represent the heat generated by appliances. As a result, the heat loads  
 308      profiles had  $15 \text{ W}\cdot\text{m}^{-2}$  from 6 am to 9 am and from 5 pm to 10 pm,  $7.5 \text{ W}\cdot\text{m}^{-2}$  from 10 pm to 6  
 309      am, and  $3.75 \text{ W}\cdot\text{m}^{-2}$  from 9 am to 5 pm. The daily distribution of the internal gains is shown in  
 310      Figure 4.

311



312

313

Figure 4. Domestic daily internal gains schedule used in this study.

314

315      2.7. *Algorithm of calculation*

316

317      The algorithm used by the model requires iteration for each time step as shown in Figure 5. Each  
 318      iteration first calculated the variable coefficients, such as the convective heat transfer coefficients  
 319      or the resistance values of the star-network. Then the temperatures of the walls, floor, and ceiling  
 320      were calculated, followed by the indoor temperature. Finally, the error between the calculated  
 321      values and the supposed values at the start of the iteration was verified. If the error was higher  
 322      than the maximum acceptable ( $10^{-6} \text{ K}$ ), a new iteration started. The supposed values were updated  
 323      with the calculated values of the previous iteration taking into account a relaxation factor. The  
 324      time step between iterations was 5 minutes.

325

326 In case the heat pump was “ON”, at the start of each iteration a temperature gradient was supposed  
327 for the supply water in each wall. At the end of each iteration, the temperature gradient was  
328 updated with the heat flux calculated for each wall.

329

330 The status of the heat pump was checked at the beginning of each time step.

331

ACCEPTED MANUSCRIPT

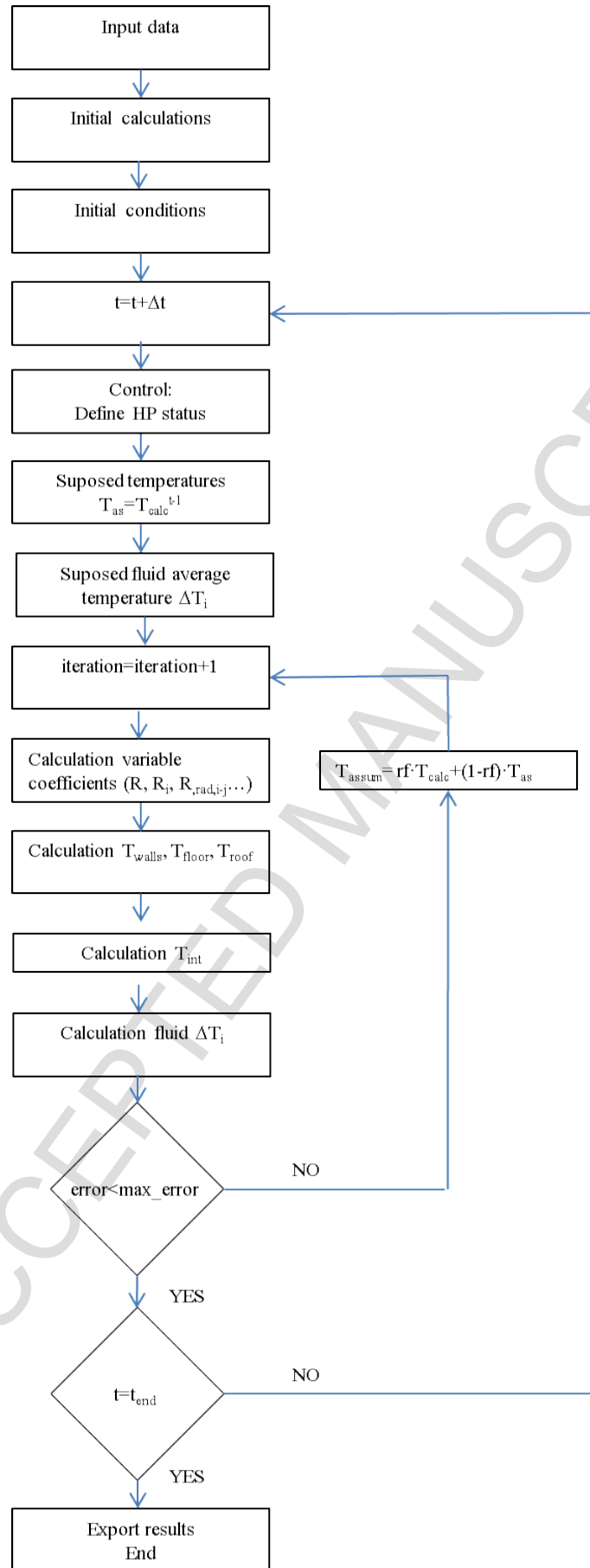


Figure 5. Model algorithm

332  
333

334

335 **3. Methodology**

336

337 *3.1. Description of control concepts*

338

339 Six control concepts were applied into the management of the heat pump, such as solar basic,  
 340 solar following, solar hybrid, solar predictive, and peak load shifting. The criterion defining each  
 341 concept depended on different objectives. First, all concepts had to maintain the indoor  
 342 temperature into the comfort range (21 °C-26 °C) all the time. Then, the different objectives were:

- 343 • To maximize the use of the energy produced by the PV panels.
- 344 • To minimize imported energy from the grid.
- 345 • To minimize imported energy from the grid in peak periods.
- 346 • To shift energy use to off-peak periods.

347

348 *3.1.1. Operation modes*

349

350 In order to achieve the objectives, each control concept used different operation modes of the heat  
 351 pump, which are described in Table 3. The mode type define its objective, with “standard” type  
 352 referring to maintaining the comfort conditions and “charging” type standing for storing energy  
 353 to the cubicle with peak load-shifting purposes.

354

355 Table 3. Heat pump operation modes (\*“Solar predictive” concept uses variable set-point for “pre-  
 356 cooling” mode)

Mode	Type	ON criterion	OFF criterion	Notes
Comfort	Standard	$T_{in} > 26\text{ °C}$	$T_{in} < 24\text{ °C}$	Always active unless another mode was ON
Solar	Charging	$T_{in} > 22\text{ °C}$	$T_{in} < 21\text{ °C}$	Only activated during daylight hours
Solar threshold	Charging	$T_{in} > 22\text{ °C}$ and $P_{PV} > 1500\text{ W}$	$T_{in} < 21\text{ °C}$ or $P_{PV} < 1500\text{ W}$	Only activated during daylight hours
Pre-cooling	Charging	$T_{in} > 22\text{ °C}^*$	$T_{in} < 21\text{ °C}^*$	Only activated in night off-peak periods

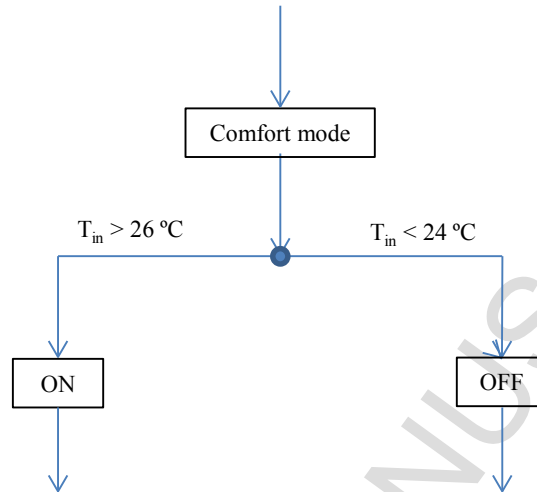
357

358 3.1.2. *No control concept*

359

360 The “no control” concept simply focused in maintaining the indoor temperature inside the comfort  
 361 range, without taking into account any other inputs. This control concept only used the “comfort”  
 362 operation mode. The scheme of the “no control” concept is shown in Figure 6.

363



364

365

Figure 6. No control concept

366

367 3.1.3. *Solar basic concept*

368

369 The “solar basic” control modified the set-point temperatures during the daylight hours with the  
 370 objective of maximizing the use of the energy produced by the PV panels. This concept had two  
 371 operation modes depending on the time. On one side “comfort mode” was activated from 6 pm  
 372 to 10 am. On the other side, “solar charging” mode was applied from 10 am to 6 pm. The scheme  
 373 of the concept is shown in Figure 7.

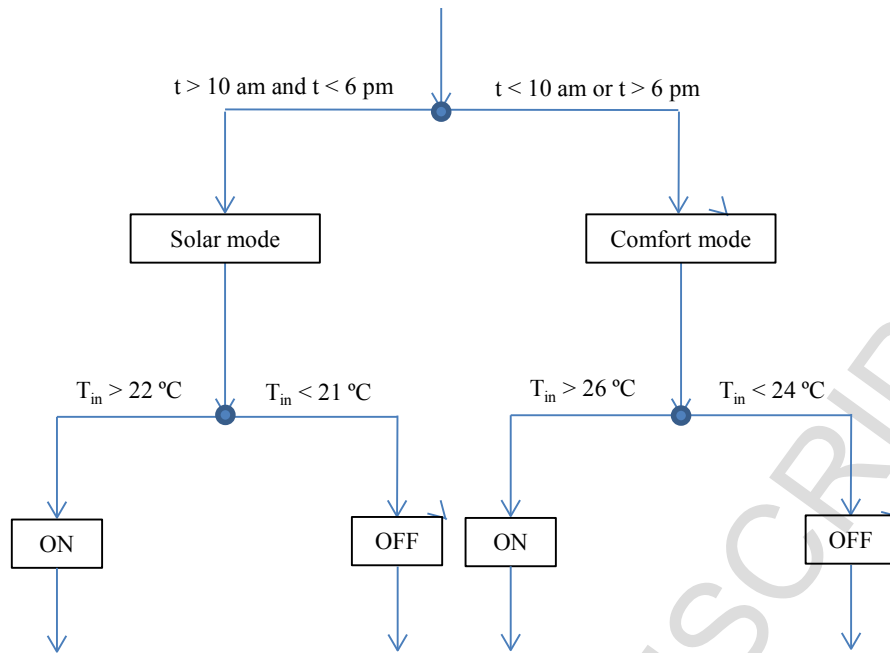


Figure 7. Solar basic control concept

374

375

376

377 *3.1.4. Solar following concept*

378

379 The “solar following” concept was a modification of the “solar basic control”. In this case the

380 actual power output of the solar panels was taken into account, activating “solar following” from

381 10 am to 6 pm. The objective of this modification was to minimize the imported energy from the

382 grid, as the concept required a solar output higher than the average power of the heat pump. If the

383 power output was insufficient, the control stayed in the “comfort” mode. The scheme of the

384 control is shown in Figure 8.

385

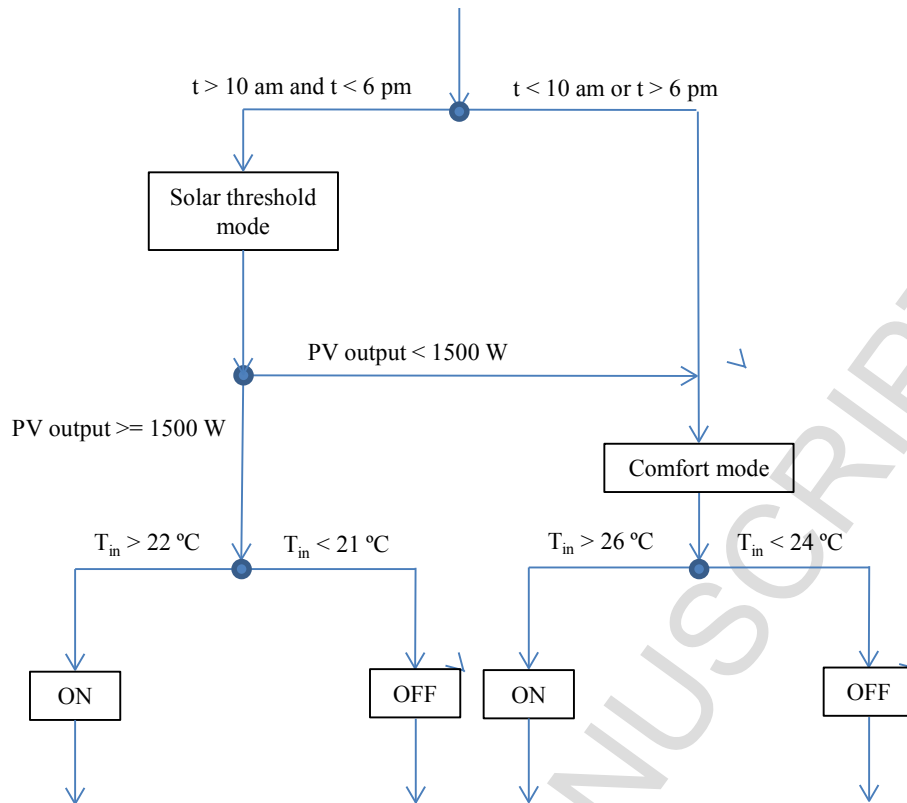


Figure 8. Solar following control concept

### 3.1.5. Solar hybrid concept

The solar hybrid concept had the objectives of maximizing the use of the energy produced by the PV panels and minimizing the imported energy in peak periods. In Spain, the change from off-peak to peak tariff is at 1 pm in summer. As a result, this concept operated in “solar” mode from 10 am to 1 pm, however, from 1 pm to 6 pm the concept operated in “solar following”. In this way, the heat pump could charge the wall during off-peak hours, exploiting the output of the PV panels even if that was not enough to off-set the energy use of the heat pump. However, once in the peak period, beyond 1 pm, the wall was charged only if the solar power output was enough, and thus the solar output was exploited but importing energy was avoided. During the rest of the day the concept operated in “comfort mode”. The scheme of the concept is shown in Figure 9.

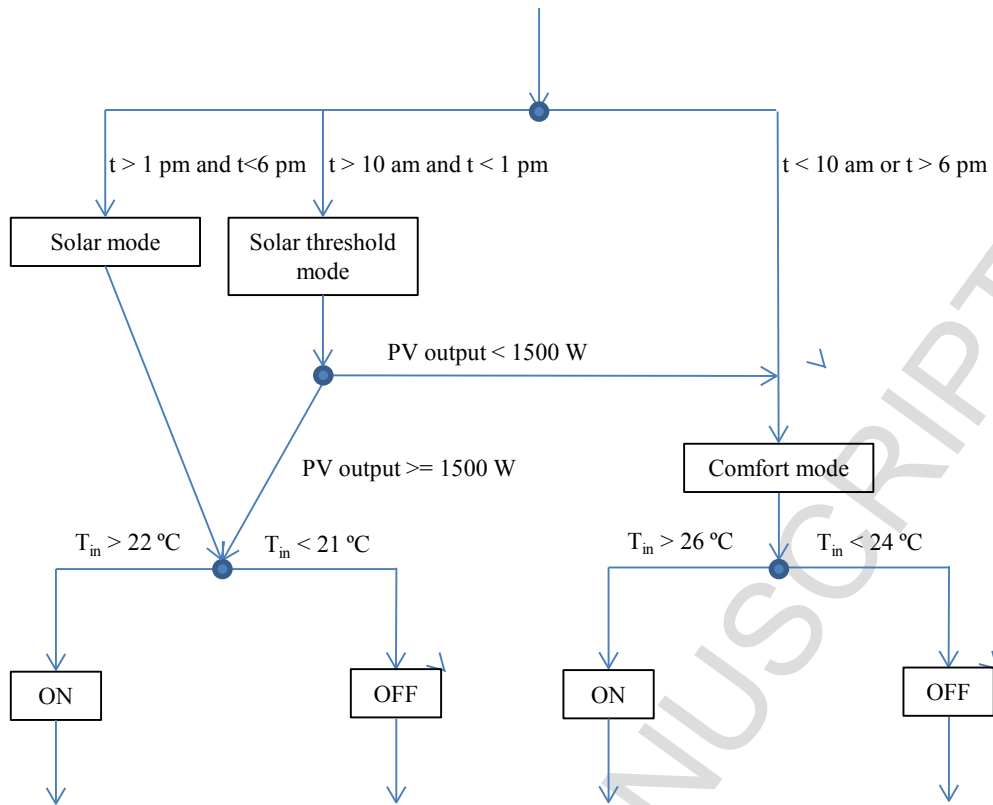


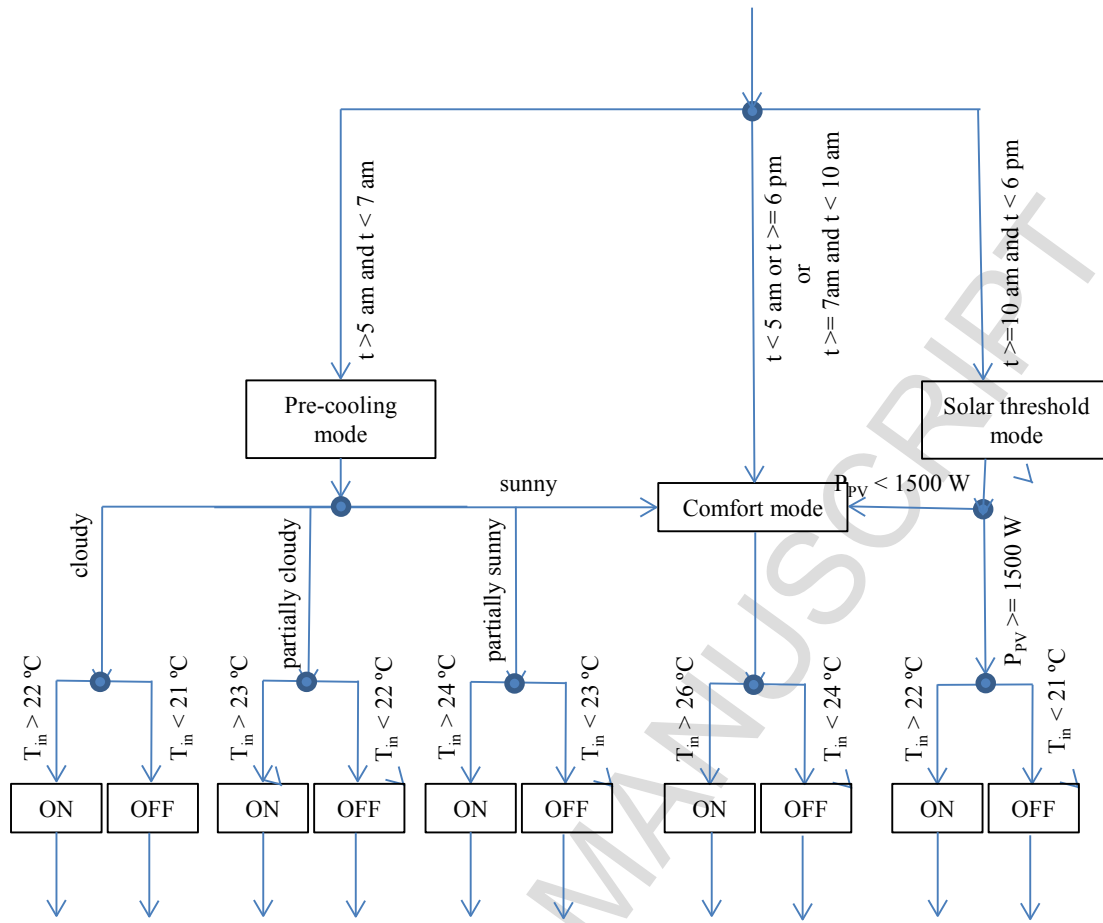
Figure 9. Solar hybrid control concept

### 3.1.6. Solar predictive concept

The objectives of the solar predictive control was to minimize the imported energy on peak periods, to maximize the use of the energy produced by the PV panels, and to shift energy use to off-peak periods. With these objectives, this concept had activated a modified “pre-cooling” mode in the early morning. In this period the control forecasted the expected solar radiation during the day, classifying it between “sunny”, “partially sunny”, “partially cloudy”, and “cloudy”. The day classification was done taking as reference the day with the highest accumulated solar radiation in the studied period, which was June 19<sup>th</sup> with a total accumulated radiation on a horizontal surface of 9.7 kWh·m<sup>-2</sup>. Then, “sunny” was considered for days with accumulated solar radiation more than 75 % of this value, “partially sunny” for values between 50-75 %, “partially cloudy” for values between 25-50 %, and “cloudy” for values below 25 %. Each type of forecasted day had different set-points in the “pre-cooling” mode, as shown in Figure 10.

Moreover, during the daylight hours, from 10 am to 6 pm, the concept operated in “solar threshold” mode. The scheme of the concept is shown in Figure 10. This concept was applied with two different length of the pre-cooling, a 2 hours period from 5 am to 7 am, and a 4 hours period from 3 am to 7 am (referred as “solar predictive 2h” and “solar predictive 4h”, respectively).

423



424

425

Figure 10. Solar predictive 2 h control concept

426

### 427 3.1.7. Peak load shifting concept

428

429 The objective of the peak load shifting concept was shifting the peak loads and minimizing the  
 430 imported energy in peak periods. As a result, it used two operation modes, “comfort” mode and  
 431 “pre-cooling” mode. Parallel to “solar predictive” concept, two different length of the pre-cooling  
 432 period were used, a 2 hours period from 5 am to 7 am, and a 4 hours period from 3 am to 7 am  
 433 (referred as “peak load shifting 2h” and “peak load shifting 4h”, respectively). The design of this  
 434 concept is an approach contrary to exploiting the PV output, as the purpose was to consume all  
 435 the energy during night-time.

436

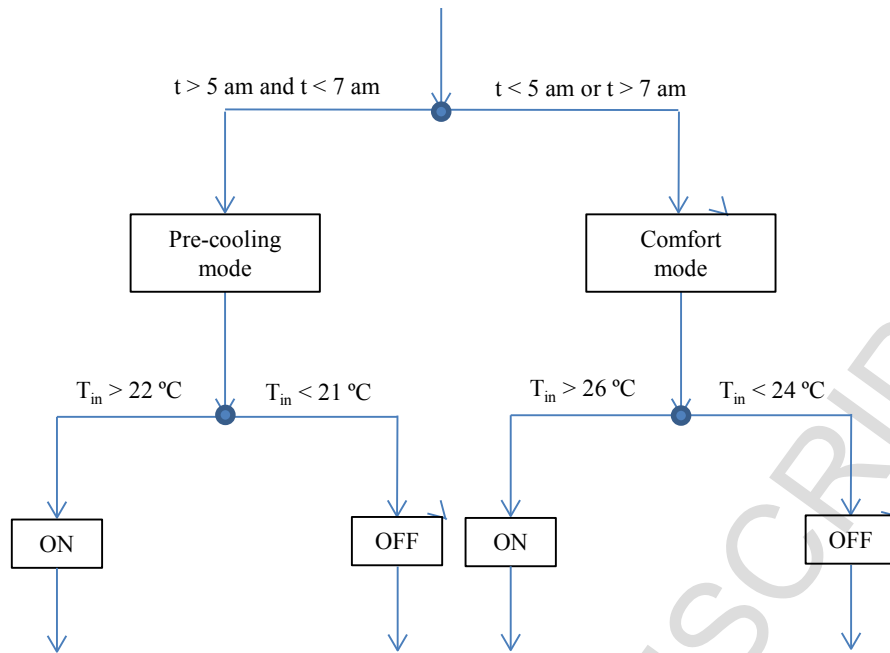


Figure 11. Peak load shifting 2 h concept

### 3.2. *Electricity cost*

Each electricity company in Spain offers different tariffs for domestic consumers, however, all tariffs take into account a peak and off peak period, which in summer peak time is from 1 pm to 11 pm. The differences between domestic tariffs are on the calculation method of the price, however, all tariffs offer incentive for the energy use in the off-peak period. A reference tariff was used in the study [33], this had a different energy cost in peak and off-peak periods, with constant power term as shown in Table 4. As the power term was constant and the research did not influence this parameter, only the energy cost was considered.

Table 4. Domestic electric tariff summary

Power term	Peak time	Peak Cost	Off peak time	Off peak cost
€/kW		€/kWh		€/kWh <sup>-1</sup>
3.17	1 pm to 11 pm	0.147675	11 pm to 1 pm	0.067255

On the other side, Spain policies promote self-consumption of the energy produced with low export prices and a tax which is payable for injecting electricity to the grid. Moreover, this study did not consider other appliances that could consume the energy produced by the PV panels. Therefore, the excess energy not consumed by the heat pump was disregarded.

456 3.3. *Weather data*

457

458 The simulations were carried out for a whole summer from May 1<sup>st</sup> to September 30<sup>th</sup>. The data  
459 were obtained from the experimental test site located at Puigverd de Lleida (Spain), whose  
460 coordinates are 41.56 N, 0.74 E. The region is considered as a hot summer and mild cold winter  
461 climate, labelled as Csa according to Köppen-Geiger [34] classification. The outdoor temperature  
462 was measured with ELEKTRONIL EE21 transducer and the solar radiation was measured with a  
463 Middleton solar pyranometer, all measurement were taken in a 5 minutes time interval.

464

465 **4. Results**

466

467 The performance of each control concept was evaluated according to the energy use, the operation  
468 cost, and the thermal comfort.

469

470 4.1. *Energy use*

471

472 The energy use for all control concepts is presented in Figure 12. The simulation results showed  
473 that all “solar” control concepts used overall more energy than “no control” or “peak-load  
474 shifting” concepts. This was caused by “solar” concepts having longer periods at low set-point,  
475 and thus higher cooling load. However, “solar” concepts had low imported energy when  
476 considering that the heat pump directly consumed the energy provided by the PV panels.

477

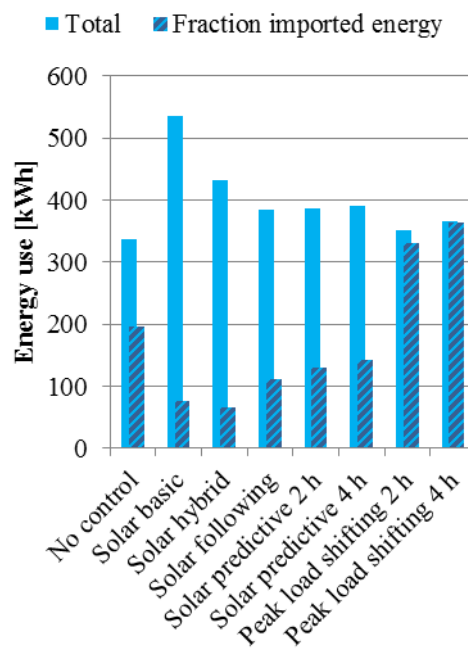
478 Among the “solar” concept, the criterion of activating the heat pump only if enough power was  
479 supplied by the PV resulted in less overall energy use but in higher imported energy. This was  
480 caused by the limited available power from the PV panels, which only had short periods providing  
481 more than 1500 W. As a result, “solar following” and “solar predictive” control concepts activated  
482 the charging mode for less time, consuming less energy. However, as fewer cooling was provided  
483 during the day time, a cooling demand was generated when internal gains kicked in at the  
484 afternoon. Then the heat pump was activated according to “comfort” mode, but without PV output  
485 available all the energy had to be imported in peak period. On the other side, “solar hybrid” had  
486 an energy use between “solar basic” and “solar following” concepts. However, once considering  
487 self-consumption “solar hybrid” had less energy use. A further advantage of “solar hybrid” was  
488 that all imported energy was consumed in off-peak periods, as shown in Figure 13. Consequently  
489 “solar hybrid” had both the least imported energy and the least peak energy use.

490

491 Furthermore, few differences were observed between “solar following” and “solar predictive”  
 492 concepts regarding overall energy use. This was mainly caused by the criterion defining the type  
 493 of days. Despite the control identified more than 25 % of days as non-sunny, and thus requiring  
 494 pre-cooling, the actual heat gains and indoor temperatures did not trigger the activation criterion  
 495 for the heat pump, as the indoor temperatures were already lower than the defined set-point.  
 496 Consequently, the energy use of “solar following” and “solar predictive” was mainly driven by  
 497 the “solar threshold” mode, which was common in both concepts. However, when considering  
 498 the distribution of the energy use, the “solar predictive” concept had more imported energy. This  
 499 was the result of the pre-cooling periods, which increased the energy use. In contrast, the pre-  
 500 cooling shifted the imported energy use to off-peak periods, resulting in “solar predictive” having  
 501 less peak energy use than “solar following”, as shown in Figure 13.

502

503 On the other side, “no control” and “peak load shifting” concepts had similar energy use, as shown  
 504 in Figure 12. However, peak load shifting concepts concentrated the energy use in off-peak  
 505 periods. Moreover, the “pre-cooling” mode schedule resulted in “peak load shifting” concepts not  
 506 exploiting the energy provided by the PV panels, therefore, importing almost all energy from the  
 507 grid. Furthermore, the different length of the pre-cooling period only resulted in a slight increase  
 508 in energy use. Otherwise, the longer period nearly guaranteed all energy use in off-peak periods.  
 509 In cooling mode, the low outdoor temperatures during the night period avoided heat gains,  
 510 therefore, once the set-point was achieved, the room did not had further cooling demand.  
 511 Consequently, the set-point was the parameter for regulating the cooling required.



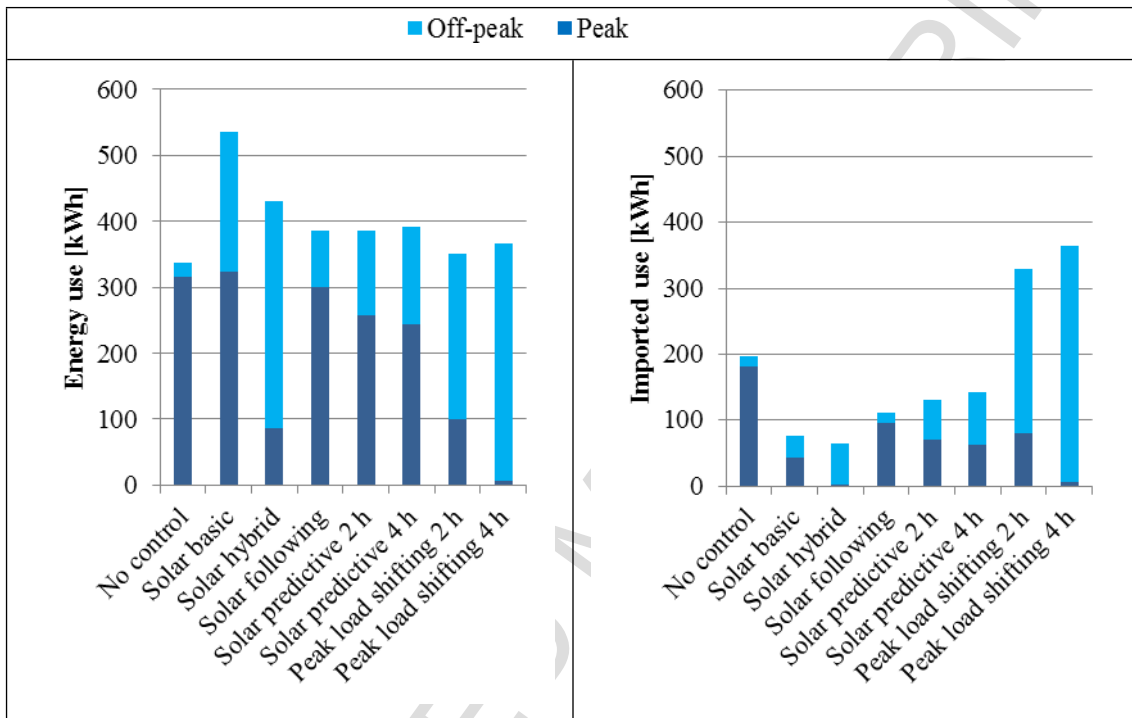
512

513

Figure 12. Total energy use and fraction of imported energy (all summer)

514

515  
516  
517  
518  
519  
520  
521  
522



523 Figure 13. Total peak and total off-peak energy use (left) and imported energy (right) (all summer)  
524

#### 525 4.2. *Operation cost*

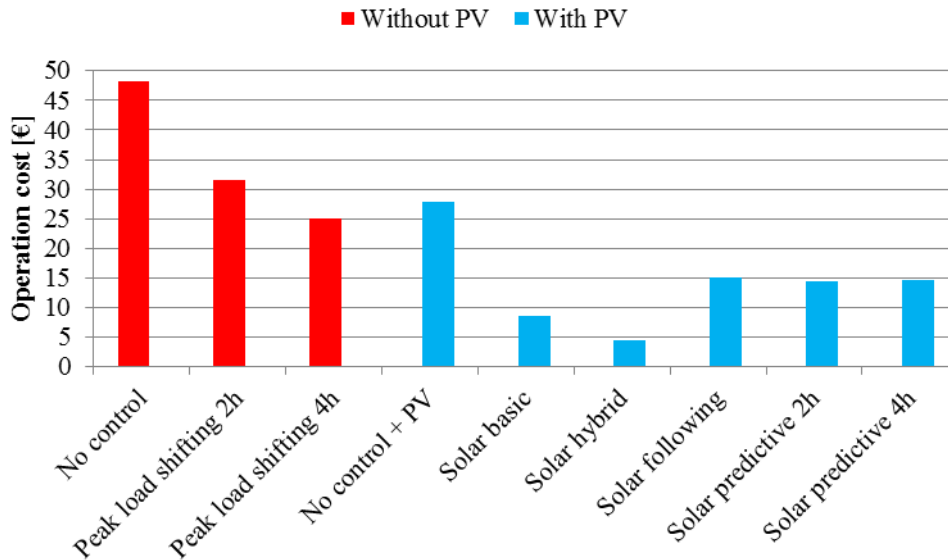
526  
527  
528  
529  
530  
531  
532  
533  
534  
535  
536

The operation costs for all control concepts are shown in Figure 14. The results are presented considering self-consumption of the PV energy output for “solar” and “no control” concepts (blue columns), although “no control” and “peak load shifting” concepts without self-consumption are shown as reference (red columns). These show that the “solar” concepts had the lowest operation cost, as a small amount of energy was imported from the grid as presented previously in Figure 13. Furthermore, as summarized in Table 5, all control concepts reduced the operation cost with self-consumption, despite this, “peak load shifting” concepts barely reduced their operation cost while “no control” reduced the cost much less than “solar” concepts. Once considering self-consumption all “solar” concepts showed high cost savings, especially the “solar hybrid” concept. Finally, the results showed that installation of PV panels was only exploited with “solar” type of

537 control concepts. “Peak-load shifting” concepts without PV achieved similar operation cost or  
 538 lower than “no control” concept with PV, therefore, the former had lower investment cost and  
 539 could also achieve lower operation costs.

540

541



542

543

Figure 14. Operation cost with and without self-consumption (all summer)

544

545

Table 5. Operation cost with self-consumption per control concept (all summer)

Control concept	Operation cost with self-consumption (€)	Control concept cost difference without and with self-consumption PV	Cost compared to “no control” with self-consumption
No control	27.87	-42.13 %	--
Solar basic	8.62	-86.12 %	- 69.08 %
Solar hybrid	4.52	-87.38 %	- 83.76 %
Solar following	15.17	-69.68 %	- 45.56 %
Solar predictive 2 h	14.38	-69.23 %	- 48.40 %
Solar predictive 4 h	14.62	-68.19 %	- 47.52 %
Peak load shifting 2 h	28.60	-9.44 %	+ 2.64 %
Peak load shifting 4 h	25.02	-0.44 %	- 10.22 %

546

547

#### 4.3. *Heat pump status*

548

549 The differences in energy use and operation cost of the “solar” control concepts can be further  
 550 understood with the heat pump operation status shown in Figure 15. The results can be  
 551 summarized as follows:

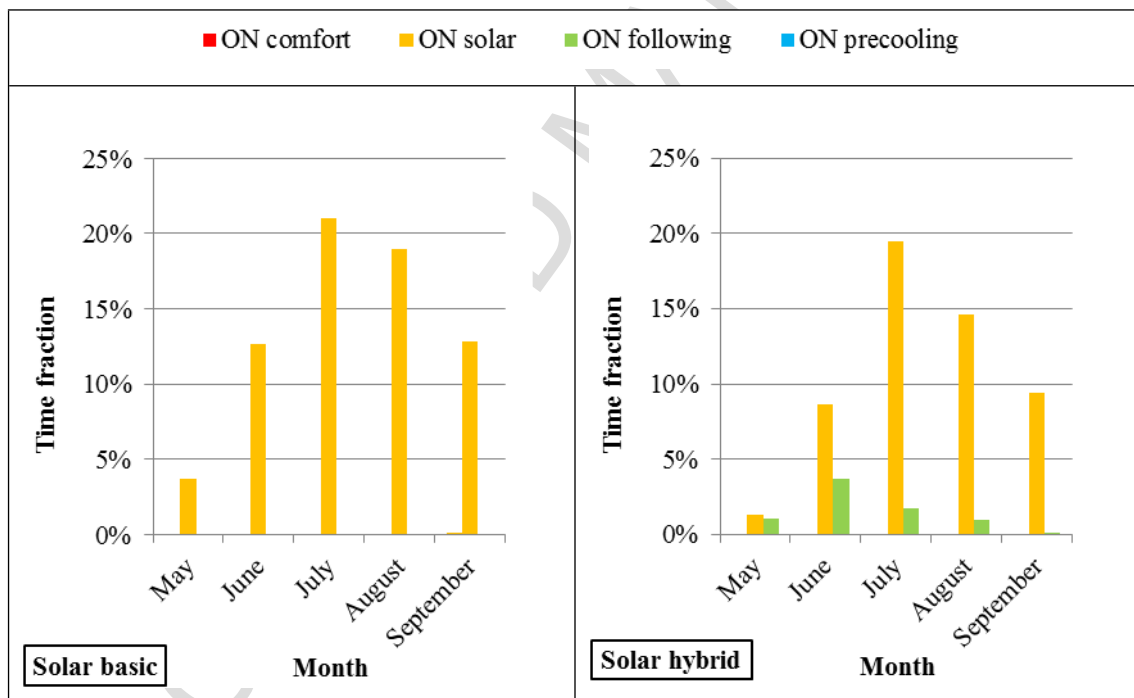
552

553 • “Solar basic” concept covered all cooling demand exclusively with “solar” mode, it did  
 554 not require turning ON in the “comfort” mode.

555 • “Solar hybrid” mainly covered the cooling demand with “solar” mode. However, as this  
 556 mode was limited up to 1 pm, the operation time of “solar hybrid” concept was lower  
 557 than “solar basic”. The remaining cooling demand was covered by “solar threshold”  
 558 mode, resulting in “solar hybrid” concept not requiring activations in “comfort” mode.

559 • “Solar following” concept did not cover all the cooling demand with “solar threshold”  
 560 mode, as the ON periods in this mode were restricted. Hence, it had to turn ON in  
 561 “comfort mode”, which was usually activated in off-peak periods during the afternoon.

562 • “Solar predictive” was similar to “solar following”, however, part of the active time in  
 563 “comfort” mode was shifted to “pre-cooling” mode, which led to lower operation cost.  
 564



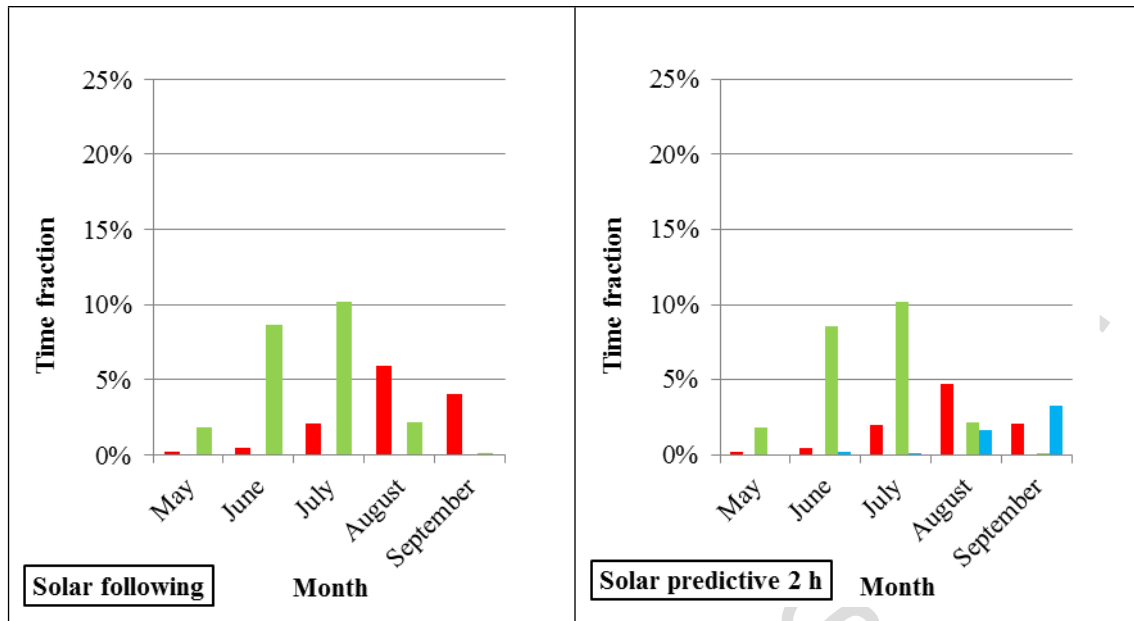


Figure 15. Time expended in each operation mode for solar control concepts

565

566

## 567 5. Discussion

568

569 The results of the study showed that the integration of radiant walls, heat pump, and PV could  
 570 significantly reduce the imported energy form the grid. By using control concepts that charge the  
 571 wall during daylight hours the system would increase the overall energy use, although, thanks to  
 572 self-consumption the imported energy would be low.

573

574 With the studied set-up, the best control concept consisted of charging during daylight hours in  
 575 off-peak periods without taking into account the actual solar output and then only charging during  
 576 peak periods if the solar power output could cover the heat pump power demand (“solar hybrid”  
 577 concept). This way the imported energy was low, moreover, all the imported energy was  
 578 consumed in off-peak periods, and thus obtaining the lowest operation cost. However, a case with  
 579 more PV installed capacity would favour a control concept in which charging is done when solar  
 580 power output exceeds heat pump power demand (“solar following” concept), as it would  
 581 guarantee zero imported energy while still having charging periods long enough.

582

583 The simulations showed the capability of the radiant wall as a TES system for storing the energy  
 584 produced by PV through a heat pump. The control concepts presented focused in minimizing the  
 585 imported energy by maximising the self-consumption of the PV output. This contrasted with  
 586 research on net-zero or net-positive energy buildings, which usually considered the grid as the  
 587 energy storage that overcame the mismatch between production and demand [11,12,15]. From a  
 588 global point of view, this approach could result in an excess of power feed to the grid during noon,

589 which would require expensive peak load shifting management at grid level that would result in  
590 higher energy cost. Consequently, focusing in maximizing self-consumption with building  
591 integrated TES, such as the radiant wall or other TABS, would both improve grid management  
592 and reduce operation cost for heating and cooling.

593

594 Despite the TES capability of the radiant walls was proven, the actual cooling performance could  
595 not be determined. Measuring the cooling supplied to the wall that actually cools down the indoor  
596 space does not reflect the behaviour of the system. While reducing the temperature resulted in an  
597 increase of the heat transferred to the wall from the outdoor space, it is also true that the radiant  
598 system acts as a thermal barrier, which reduces heat gains to the interior space. Furthermore, the  
599 focus of this research was to charge the wall with solar energy, and even with increased heat gains  
600 the operation cost and associated greenhouse emissions are very low. In the case studied here, the  
601 thermal efficiency of the radiant wall is a less relevant parameter compared to the increase of  
602 renewable energy use.

603

604 However, fully exploiting TABS storage capacity requires optimized controls. The literature  
605 presents extensive research on TABS control [6,8], among which predictive controls showed good  
606 synergy with TABS [8]. On this topic, the results on the studied control concepts offered  
607 guidelines towards improving predictive controls performance, by indicating the general control  
608 parameters to consider in the cost functions. Moreover, this paper presents an intuitive approach  
609 to best control, although it also highlights some key parameters to optimize such as indoor  
610 temperature set-point, PV output threshold for activating the heat pump, forecasting of PV output,  
611 expected cooling load and start/end time for charging periods. These parameters should be  
612 managed in order to minimize the operation cost and the imported energy while being constrained  
613 by the indoor temperature comfort range.

614

615 Furthermore, the presented research considered an air-to-water heat pump supplying at constant  
616 temperature and constant flow. Adjustment of these parameters could lead to a better performance  
617 of the heat pump [17], and consequently resulting in less overall energy use and operation cost.  
618 Moreover, using outdoor air as a heat sink meant a worse heat pump COP when charging during  
619 the day, as the outdoor temperature was higher. A ground source heat pump, free-cooling with  
620 ground heat exchanger, or evaporatively cooled condenser could improve the system performance  
621 in cooling mode, further increasing the advantage of “solar” concepts.

622

623 Finally, the results suggest moving away from the usual energy efficiency approach. The control  
624 concepts with less imported energy and operation cost were those consuming more overall energy.  
625 This is a common issue in peak load shifting with TES [16], which present benefits by increasing

626 the renewable energy share although having higher overall energy use. In a context in which PV  
627 panels are getting cheaper [35] the feasibility of big PV arrays is higher, especially in single family  
628 houses. Consequently, solar electricity could be abundant, and thus the challenge will be to better  
629 exploit this energy, with energy efficiency being one parameter of the optimization process.

630

## 631 **6. Conclusions**

632

633 The control of a system consisting of radiant wall as TES for a heat pump coupled to a PV array  
634 was studied. Different control concepts were considered with the objective to reduce operation  
635 cost by peak load shifting, minimization of imported electricity from the grid, and maximisation  
636 of PV energy use. An experimentally validated model of a radiant wall was coupled to a simple  
637 room model that provided a base case for studying the behaviour of the different control concepts.

638

639 Charging the radiant wall with the solar energy output of a PV array through a heat pump resulted  
640 in a higher overall energy use. However, due to self-consumption of the produced energy the  
641 system imported little energy from the grid, resulting in a low operation cost.

642

643 The simulations also highlighted some parameters that could be optimized, such as indoor  
644 temperature set-point, PV output threshold for activating the heat pump, forecasting of PV  
645 production, expected cooling load and length and timing of charging periods.

646

647 The solar control concepts were promising references for reducing operation cost and minimizing  
648 imported energy. These were a solid base for the research of optimized control strategies of a  
649 radiant wall used as TES for a heat pump coupled to a PV array.

650

## 651 **7. Acknowledgements**

652

653 The authors acknowledge the South Australian Department of State Development who have  
654 funded this research through the Premier's Research Industry Fund - International Research Grant  
655 Program (IRGP 33). The work was partially funded by the Spanish government (ENE2015-  
656 64117-C5-1-R (MINECO/FEDER), ENE2015-64117-C5-3-R (MINECO/FEDER), and  
657 ULLE10-4E-1305). GREA is certified agent TECNIO in the category of technology developers  
658 from the Government of Catalonia. The authors would like to thank the Catalan Government for  
659 the quality accreditation given to their research group (2014 SGR 123) and the city hall of  
660 Puigverd de Lleida. This projects has received funding from the European Commission Seventh

661 Framework Programme (FP/2007-2013) under Grant agreement N° PIRSES-GA-2013-610692  
662 (INNOSTORAGE) and from European Union's Horizon 2020 research and innovation  
663 programme under grant agreement N° 657466 (INPATH-TES). Alvaro de Gracia would like to  
664 thank Ministerio de Economía y Competitividad de España for Grant Juan de la Cierva, FJCI-  
665 2014-19940.

666        **References**

- 667    1.    International Energy Agency, Energy Technology Perspectives 2012 Pathways to a clean  
668        energy System, 2012
- 669    2.    European Commission, Technical Guidance-Financing the energy renovation of building  
670        with Cohesion Policy Funding, 2014
- 671    3.    DIRECTIVE 2010/31/EU of European parliament and of the council of 18May 2010 on the  
672        energy performance of buildings (recast)
- 673    4.    United Nations, Adoption of the Paris Agreement, Paris Climate Change Conference COP  
674        21, UN, 2015
- 675    5.    X. Xu, S. Wang, J. Wang, F. Xiao, Active pipe-embedded structures in buildings for  
676        utilizing low-grade energy sources: A review, *Energy Build.*, 42 (2010) 1567–1581
- 677    6.    J. Romani, A. de Gracia, L.F. Cabeza, Simulation and control of thermally activated  
678        building systems (TABS), *Energy Build.*, 127 (2016) 22-42
- 679    7.    K.N. Rhee, B.W. Olesen, K.W. Kim, Ten questions about radiant heating and cooling  
680        systems, *Build. Env.* 112 (2017) 367-381
- 681    8.    D. Olsthoorn, F. Haghghat, A. Moreau, G. Lacroix, Abilities and limitations of thermal  
682        mass activation for thermal comfort, peak shifting and shavings: A review, *Build. and Env.*  
683        118 (2017) 113-127
- 684    9.    J. Romani, G. Pérez, A. de Gracia, Experimental evaluation of a cooling radiant Wall  
685        coupled to a ground heat exchanger, *Energy Build.* 129 (2016) 484-490
- 686    10. R.A. Meierhans, Room air conditioning by means of overnight cooling of the concrete  
687        ceiling, *ASHRAE Trans.* 102 (1996) 693-69
- 688    11. M. Bakker, H.A. Zondag, M.j. Elswijk, K.J. Strootman, M.J.M. Jong, Performance and  
689        costs of a roof-sized PV/thermal array combined with ground coupled heat pump, *Sol.*  
690        *Energy* 78 (2005) 331-339
- 691    12. M. Bojic, N. Nikolic, D. Nikolic, J. Skerlic, I. Miletic, Toward a positive-net-energy  
692        residential building in Serbian conditions, *Appl. Energy* 88 (2011) 2407-2419
- 693    13. J.A. Candanedo, A.K. Athienitis, Predictive control of radiant floor heating and solar-  
694        source heat pump operation in a solar house, *HVAC R. Res* 17 (3) (2011) 235-256

- 695 14. S. Li, J. Joe, J. Hu, P. Karava, System identification and model predictive control of office  
696 building with integrated photovoltaic thermal collectors, radiant floor heating and active  
697 thermal storage, *Sol. Energy* 113 (2015) 139-157
- 698 15. G.A. Dávi, E. Caamaño-Martín, R. Rüter, J. Solano, Energy performance evaluation of a  
699 net plus-energy residential building with grid-connected photovoltaic system in Brazil,  
700 *Energy Build.* 120 (2016) 19-29
- 701 16. A. Arteconi, E. Ciarrocchi, Q. Pan, F. Carducci, G. Comodi, Thermal energy storage with  
702 PV panels for demand side management of industrial building cooling loads, *Appl. Energy*  
703 185 (2017) 1984-1993
- 704 17. A.K. de Wit, C.J. Wisse, Hydronic topologies for thermally activated building systems –  
705 design questions and case study, *Energy Build.* 52 (2012) 56-67
- 706 18. S.-H Cho, M. Zaherr-uddin, An experimental study of multiple parameter switching control  
707 for radiant floor heating systems, *Energy* 24 (1999) 433-444
- 708 19. M. Krzaczek, Z. Kowalczyk, Gain scheduling control applied to thermal barrier in systems  
709 of indirect passive heating and cooling of buildings, *Control Eng.* 20 (2012) 1325-1336
- 710 20. M. Gwerder, J. Tödli, B. Lehmann, V. Dorer, W. Güntensperger, F. Renggli, Control of  
711 thermally activated building systems (TABS) in intermittent operation with pulse width  
712 modulation, *Appl. Energy* 86 (2009) 1606-1616
- 713 21. M. Schmelas, T. Feldmann, E. Bollin, Adaptive predictive control of thermo-active  
714 building systems (TABS) based on a multiple regression algorithm, *Energy Build.* 103  
715 (2015) 14-28
- 716 22. S. Privara, J. Siroky, I. Ferkl, J. Cigler, Model predictive control of a building heating  
717 system: the first experience, *Energy Build.* 42 (2011) 564-572
- 718 23. B.W. Olesen, K. Sommer, B. Ditching, Control of slab heating and cooling systems studied  
719 by dynamic computer simulations, *ASHRAE Trans.* 108 (2) (2000) 698-707
- 720 24. J. Romani, G. Pérez, A. de Gracia, Experimental evaluation of a cooling radiant Wall  
721 coupled to a ground heat exchanger, *Energy Build.* 129 (2016) 484-490
- 722 25. J. Romani, G. Pérez, A. de Gracia, Experimental evaluation of a heating radiant wall  
723 coupled to a ground source heat pump, *Renew. Energy* 105 (2017) 520-529

- 724 26. J. Romani, L.F. Cabeza, A. de Gracia, Development and experimental validation of a  
725 transient “D numeric model for radiant walls, Submitted to Renew. Energy (June 2017)
- 726 27. EN ISO 6946 (2007), Building components and building elements – Thermal resistance  
727 and thermal transmittance – Calculation method
- 728 28. J.E. Seem, Modeling of heat transfer in Buildings, 1987, University of Wisconsin-  
729 Madison:Madison
- 730 29. G. Gebhart , Heat transfer, Second Edition, McGraw-Hill, (1971) 150-158
- 731 30. W.C. Swinback, Q.J. Roy, Long-wave radiation from clear skies, Q.J.R Meteorol, Soc.89  
732 (1936) 339
- 733 31. S. Joan, D. Baggs, Australian earth-covered and green roof building 3rd ed. 2009: Dual  
734 Harmony publications
- 735 32. BITZER, <https://www.bitzer.de> (accessed June 2017)
- 736 33. ENDESA, <https://www.endesaclientes.com/> (accessed June 2017)
- 737 34. M. Kottek, J. Grieser, C. Beck, B. Rudolf, F. Rubel, World map of Köppen-Geiger climate  
738 classification updated, Meteorol. Zeitschrift, 15 (2) (2006) 259-263
- 739 35. G.L. Barbose, N.R. Darghouth, Tracking the Sun IX: The installed price of residential and  
740 non-residential photovoltaic systems in the United States, CA. Lawrence Berkeley National  
741 Laboratory (2016)
- 742